

# The Contribution of the First Stars to the Cosmic Infrared Background

Michael R. Santos,<sup>1</sup> Volker Bromm<sup>2</sup> and Marc Kamionkowski<sup>1</sup>

<sup>1</sup>*California Institute of Technology, Mail Code 130-33, Pasadena, CA 91125, U.S.A.*

<sup>2</sup>*Harvard-Smithsonian Center for Astrophysics, 60 Garden Street, Cambridge, MA 02138, U.S.A.*

30 October 2018

## ABSTRACT

We calculate the contribution to the cosmic infrared background from very massive metal-free stars at high redshift. We explore two plausible star-formation models and two limiting cases for the reprocessing of the ionizing stellar emission. We find that Population III stars may contribute significantly to the cosmic near-infrared background if the following conditions are met: (i) The first stars were massive, with  $M \gtrsim 100 M_{\odot}$ . (ii) Molecular hydrogen can cool baryons in low-mass haloes. (iii) Pop III star formation is ongoing, and not shut off through negative feedback effects. (iv) Virialized haloes form stars at about 40 per cent efficiency up to the redshift of reionization,  $z \sim 7$ . (v) The escape fraction of the ionizing radiation into the intergalactic medium is small. (vi) Nearly all of the stars end up in massive black holes without contributing to the metal enrichment of the Universe.

**Key words:** cosmology: theory – early Universe – galaxies: formation – stars: formation – diffuse radiation – infrared: general.

## 1 INTRODUCTION

It has long been realized that observations of the cosmic infrared background (CIRB) can place important constraints on the energy production associated with the formation of cosmological structure (see Hauser & Dwek 2001 and references therein). The cosmic background is the locally measured radiation density from all extragalactic sources. Starlight dominates the CIRB in the near-IR, whereas the mid- and far-IR backgrounds result primarily from dust emission (e.g., Dwek et al. 1998).

Observational efforts to measure the near-IR CIRB are hampered by strong and uncertain foreground contamination from zodiacal dust. Cambr sy et al. (2001), using data from the Diffuse Infrared Background Experiment (DIRBE) on the *COBE* satellite, found that the integrated light from all galaxies (estimated from deep surveys) is not sufficient to account for the measured CIRB at  $1.25 \mu\text{m}$  (*J* band) or  $2.2 \mu\text{m}$  (*K* band). Wright & Johnson (2001) analyzed the same DIRBE data as Cambr sy et al. (2001), but subtracted a different zodiacal light model; they find a *J*-band CIRB that is consistent with the contribution from galaxies, but their *K*-band CIRB value is larger than the background inferred from galaxy counts. Totani et al. (2001) model the contribution from galaxies missed by deep galaxy surveys and find that it is unlikely to be greater than 30 per cent of the measured light.

Bond, Carr & Arnett (1986) suggested that the first

generation of stars in the Universe, called Population III (Pop III) stars because they are assumed to have near-zero metallicity, may contribute significantly to the cosmic background. The cosmological impact of Pop III stellar radiation has been addressed before (e.g., Carr, Bond & Arnett 1984; Bond et al. 1986; Couchman & Rees 1986; Haiman & Loeb 1997; Ciardi et al. 2001). Recent theoretical advances have improved our understanding of the physics of Pop III star formation (see Barkana & Loeb 2001 and references therein); in particular, three-dimensional numerical simulations suggest that the primordial initial mass function (IMF) may have been concentrated at stellar masses  $\gtrsim 100 M_{\odot}$  (Bromm, Coppi & Larson 1999, 2002; Abel, Bryan & Norman 2000). Stars with masses  $\gtrsim 100 M_{\odot}$ , which we will call ‘very massive’ (Carr et al. 1984), have spectra and luminosities that asymptotically approach the blackbody form and the Eddington limit, respectively (e.g., Bromm, Kudritzki & Loeb 2001b).

In this paper, we investigate whether a significant fraction of the near-IR CIRB may come from very massive Pop III stars. Since these stars are very luminous per unit stellar mass over a short lifetime, they may contribute substantially to the CIRB. We use two different models for the formation of dark matter (DM) haloes to calculate the rate at which baryons are processed through haloes with virial temperatures high enough to allow baryonic cooling (§2). In addition, we consider two possibilities for the re-processing of the stellar emission by the gas in the halo and by the

intergalactic medium (§3). In §4 we show our model results and the observational data. Section 5 contains a discussion of our results and compares them with the data.

We adopt the following values for the cosmological parameters:  $h = 0.7$ ,  $\Omega_m = 0.3$ ,  $\Omega_\Lambda = 0.7$ ,  $\Omega_B h^2 = 0.019$ ,  $\sigma_8 = 0.9$ . Here  $h$  is the dimensionless Hubble constant,  $H_0 = 100h \text{ km s}^{-1} \text{ Mpc}^{-1}$ ;  $\Omega_m$ ,  $\Omega_\Lambda$  and  $\Omega_B$  are the total matter, cosmological constant and baryon density in units of the critical density and  $\sigma_8$  gives the normalization of the power spectrum on the  $8h^{-1} \text{ Mpc}$  scale.

## 2 STAR-FORMATION RATE

### 2.1 Overview of the star-formation model

We assume that the star-formation rate (SFR) of Pop III stars is related to the cooling of baryons in collapsed dark-matter haloes (henceforth just ‘haloes’). The cooling rate of baryons is a very strong function of baryon temperature near certain temperature thresholds: above these thresholds a new cooling mechanism can act within the gas. For a given choice of cooling mechanism, we would like to calculate the rate at which baryons are heated above the associated temperature threshold, and thus may collapse to high density and form stars.

If baryons in a halo are shock-heated to the virial temperature of their halo, the temperature of those baryons is related to the mass of that halo according to  $T \propto M^{2/3}$ . So as a proxy for the temperature history of the baryons, we may calculate the mass history of haloes, assuming a constant ratio of baryonic matter to dark matter in all haloes, and that baryons below the cooling threshold are always heated to the virial temperature of their halo. In this picture haloes above a critical mass may form stars, because those haloes have heated their gas above the critical temperature, and haloes below the critical mass do not form any stars. Additionally, we parametrize the fraction of eligible baryons that actually do form stars with a constant star formation efficiency,  $\eta$ .

The mass-assembly history of dark-matter haloes is computed using the extended Press-Schechter formalism (Lacey & Cole 1993), where the  $\sigma(M)$ – $M$  relation is evaluated with the power spectrum of Eisenstein & Hu (1999). Here  $\sigma(M)$  is the standard deviation of the linear density field smoothed on scales containing a mean mass  $M$ . Our choices of  $M_{\text{crit}}(z)$  are described in §2.3.

We consider two models for the SFR. In both models, star formation is triggered in a halo as it accumulates enough mass to put it above the threshold mass  $M_{\text{crit}}(z)$ , but the models differ in how they treat additional material that merges into such haloes. In the ‘ongoing’ model, all gas in haloes with  $M \geq M_{\text{crit}}(z)$  is eligible for star formation. Conversely, the ‘single-burst’ model only allows star formation in haloes that have not previously formed stars and have no progenitor halo that has formed stars, i.e., both merging haloes are crossing the critical threshold for the first time.

### 2.2 Specific star-formation models

#### 2.2.1 Ongoing star formation

In the ongoing model, the SFR in a single halo is proportional to the growth (in mass) of that halo, after it has be-

come more massive than  $M_{\text{crit}}(z)$ . Star formation does not occur in a quiescently evolving (i.e., non-accreting) halo; the star formation is not *continuous* in the usual sense. But star formation is not inhibited after the first generation of Pop III stars is born in a halo, which assumes that radiation and mechanical outflows from the life and death of the star(s) have no impact (zero feedback) on future star formation.

The SFR in the ongoing model is proportional to the time derivative of the total mass contained in haloes that have mass  $M \geq M_{\text{crit}}(z)$ . The SFR per comoving volume,  $\psi_{\text{on}}$ , is

$$\psi_{\text{on}}(z, M_{\text{crit}}(z)) = \eta \frac{\Omega_B}{\Omega_m} \frac{d}{dt} \int_{M_{\text{crit}}(z)}^{\infty} dM M \frac{dn_{\text{PS}}}{dM}(M, z). \quad (1)$$

Here  $n_{\text{PS}} \equiv n_{\text{PS}}(M, z)$  is the comoving number density of haloes of mass  $M$  at redshift  $z$ , given by Press & Schechter (1974). The integral expresses the collapsed mass per comoving volume contained in haloes above the critical mass. The time derivative converts this to a mass rate, and the prefactors convert from total mass to stellar mass.

#### 2.2.2 Single-burst star formation

In the single-burst model, a halo forms stars when the accretion of matter pushes its mass above the critical mass,  $M_{\text{crit}}(z)$ ; that is the only time that the halo will form stars, regardless of additional mergers and mass accretion. This is a very extreme model which assumes Pop III stars make a long-term change in their surroundings which permanently prohibits future Pop III stars from forming there. This extreme model could be realistic if Pop III stars heavily enrich the interstellar medium with metals. Then, though stars will likely eventually form out of that material, Pop III stars will not. The SFR may lie somewhere between the prediction of this model, and the prediction of the ongoing model discussed above (in which all baryons in haloes with  $M > M_{\text{crit}}(z)$  are eligible to form stars).

The SFR in the single-burst model can be calculated with the extended Press-Schechter formalism: A halo grows in mass through discrete mergers and gradual accretion, which is treated as a series of small mergers in extended Press-Schechter theory. As an example, take a halo with mass  $M_1$  at some redshift  $z$  that merges with mass  $\Delta M$  for a total mass of  $M_2 = M_1 + \Delta M$  at redshift  $z + dz$ , where  $dz$  is small and negative, i.e., a short time later. If  $M_1 < M_{\text{crit}}(z)$  and  $M_2 \geq M_{\text{crit}}(z)$ , then, provided  $\Delta M < M_{\text{crit}}(z)$ , the halo undergoes a burst of star formation. We parametrize the mass of stars formed,  $M_*$ , by

$$M_* = \eta \frac{\Omega_B}{\Omega_m} M_2. \quad (2)$$

The SFR per comoving volume,  $\psi_{\text{burst}}$ , is

$$\psi_{\text{burst}}(z, M_{\text{crit}}(z)) = \frac{1}{2} \frac{\eta \Omega_B}{\Omega_m} \times \int_0^{M_{\text{crit}}(z)} dM_1 \frac{dn_1}{dM_1} \int_{M_{\text{crit}}(z)}^{M_{\text{crit}}(z)+M_1} dM_2 M_2 \frac{d^2 P}{dM_2 dt}, \quad (3)$$

where  $n_1 \equiv n_{\text{PS}}(M_1, z)$  and  $P \equiv P(M_1, M_2, z)$  is the probability that a halo with mass  $M_1$  merges to a new mass

$M_2 > M_1$  at redshift  $z$  (Lacey & Cole 1993). The prefactor of 1/2 corrects for double counting in the integrals (for fixed  $M_1$  and  $\Delta M$ , the integral as written counts both  $M_1 + \Delta M = M_2$  and  $\Delta M + M_1 = M_2$ ).<sup>\*</sup> A similar approach to model the history of star formation at high redshifts has been discussed by Barkana & Loeb (2000).

### 2.3 Critical halo mass for star formation

There is a relationship between the mass of a halo and its virial temperature. Using the assumptions we made in §2.1, we can substitute a critical temperature for baryonic cooling,  $T_{\text{crit}}$ , into that relation to find the corresponding critical mass:

$$M_{\text{crit}}(z) = 0.94 \times 10^8 M_{\odot} \left(\frac{h}{0.7}\right)^{-1} \left(\frac{\Omega_m}{0.3}\right)^{-1/2} \times \left(\frac{1+z}{10}\right)^{-3/2} \left(\frac{\mu}{0.6}\right)^{-3/2} \left(\frac{T_{\text{crit}}}{10^4 \text{ K}}\right)^{3/2}, \quad (4)$$

where  $\mu$  is the mean molecular weight ( $\mu = 0.6$  for ionized gas [ $T_{\text{crit}} \gtrsim 10^4$  K] and  $\mu = 1.2$  for neutral gas [ $T_{\text{crit}} \lesssim 10^4$  K]) (Barkana & Loeb 2001).

We seek to model only two cooling processes: radiative cooling from molecular hydrogen and radiative cooling from atomic hydrogen. For molecular cooling, we choose  $T_{\text{crit}} = 400$  K (e.g., Tegmark et al. 1997; Abel et al. 1998). For atomic cooling, we choose  $T_{\text{crit}} = 10^4$  K (Barkana & Loeb 2001).

### 2.4 Limits on the abundance of Pop III stars

A realistic model of Pop III star formation must conform to some observational constraints. The matter density processed through Pop III stars as a fraction of the critical density is

$$\Omega_{\text{III}}(z) = \frac{1}{\rho_c} \int_z^{\infty} \psi(z') \left| \frac{dt'}{dz'} \right| dz', \quad (5)$$

with

$$\left| \frac{dt}{dz} \right| = [H_0(1+z)E(z)]^{-1},$$

and, in a flat universe,

$$E(z) = [\Omega_m(1+z)^3 + \Omega_{\Lambda}]^{1/2}.$$

Here,  $\psi$  is the SFR and  $\rho_c$  is the density required to close the Universe. A strong upper limit on  $\Omega_{\text{III}}$  is that it must not exceed  $\Omega_B$ . Below we discuss two constraints on the possible products of Pop III stars, black holes and heavy elements (see also Schneider et al. 2002).

#### 2.4.1 Black holes

A nonrotating star with mass above  $\sim 260 M_{\odot}$  is predicted to evolve directly to a black hole without any metal ejection (Fryer, Woosley & Heger 2001). The fate of rotating stars in that mass range is unknown, but may be similar.

<sup>\*</sup> There is some ambiguity in the SFR arising from the extended Press-Schechter merger rates. We defer discussion of that to future work, and here evaluate the SFR as written.

If so, and if the Pop III IMF were concentrated at masses above  $\sim 260 M_{\odot}$ , most of the baryons once in Pop III stars would now be in black holes. Such black holes would populate the halo of our galaxy, but they would be very difficult to detect unless they have a companion; e.g., the MACHO microlensing study places no constraint on the fraction of the Milky Way halo contained in  $\gtrsim 100 M_{\odot}$  black holes (Alcock et al. 2001). Detailed theoretical studies may eventually reveal the fraction of such black holes that currently have a companion object, and searches for those binary systems, or future microlensing studies, could lead to constraints on  $\Omega_{\text{BH}}$  (e.g., Agol & Kamionkowski 2001). But currently even if  $\Omega_{\text{BH}} = \Omega_{\text{III}}$  there is no additional constraint on  $\Omega_{\text{III}}$  from limits on black holes.

#### 2.4.2 Metal enrichment

A nonrotating star with mass between  $\sim 140 M_{\odot}$  and  $\sim 260 M_{\odot}$  is expected to end its evolution in a pair-instability supernova, which completely disrupts the star and leaves no remnant (Heger & Woosley 2002). In this case all of the nucleosynthetic products of the star are ejected, and potentially pollute the intergalactic medium (IGM) (cf. §2.4.1, where all were swallowed into a black hole). Thus metal abundances in the Universe, especially at high redshift, are limited on the number of Pop III stars which resulted in supernovae, given assumptions about the mixing of the metals.

If a fixed fraction  $\epsilon_{\text{pi}}$  (‘pi’ for ‘pair instability’) of the mass converted into Pop III stars is expelled in pair-instability supernovae, the nucleosynthetic yield calculation from Heger & Woosley (2002) may be used to determine the contribution from Pop III stars to the metallicity of the IGM. For

$$[i] \equiv \log_{10} \left( \frac{f_i^U}{f_i^{\odot}} \right), \quad (6)$$

where  $i$  is a species and  $f_i^U$  and  $f_i^{\odot}$  are the mass fractions of species  $i$  in the Universe and Sun, respectively. Similarly, if we denote the ejected mass fraction of species  $i$  by  $f_i^E$ , then

$$f_i^U = \epsilon_{\text{pi}} \frac{\Omega_{\text{III}}}{\Omega_B} f_i^E \quad (7)$$

and

$$[i] = \log_{10} \left( \epsilon_{\text{pi}} \frac{\Omega_{\text{III}}}{\Omega_B} P_i \right), \quad (8)$$

where  $P_i \equiv f_i^E / f_i^{\odot}$  is the production factor of species  $i$ . Heger & Woosley (2002, table 4) calculated  $P_i$  for many isotopes and stellar masses. We here take  $\sim 200 M_{\odot}$  as a fiducial mass for a pair-instability supernova progenitor.

A few values of interest from their table are  $P_i(i = {}^{12}\text{C}, {}^{16}\text{O}, {}^{24}\text{Mg}, {}^{28}\text{Si}, {}^{56}\text{Fe}) = (13.2, 45.8, 85.7, 353, 49.8)$ . In general, the highest values of  $P_i$  are for the alpha elements.

Observations of the abundance of species  $i$  in the high-redshift universe are sometimes quoted in slightly different notation from  $[i]$ . Assuming  $\epsilon_{\text{pi}} \Omega_{\text{III}} \ll \Omega_B$ ,  $[i/\text{H}] \simeq [i]$ . Using tabulated values for  $f_i^E$  (Heger & Woosley 2002, table 3), it is straightforward to calculate  $\Omega_i = f_i^U \Omega_B$ . With assumptions about the mixing of the ejecta from Pop III stars, measurements of metals in the IGM at high redshifts (or the metallicities of stars formed at high redshifts) can place a limit on a combination of the IMF of Pop III stars (which

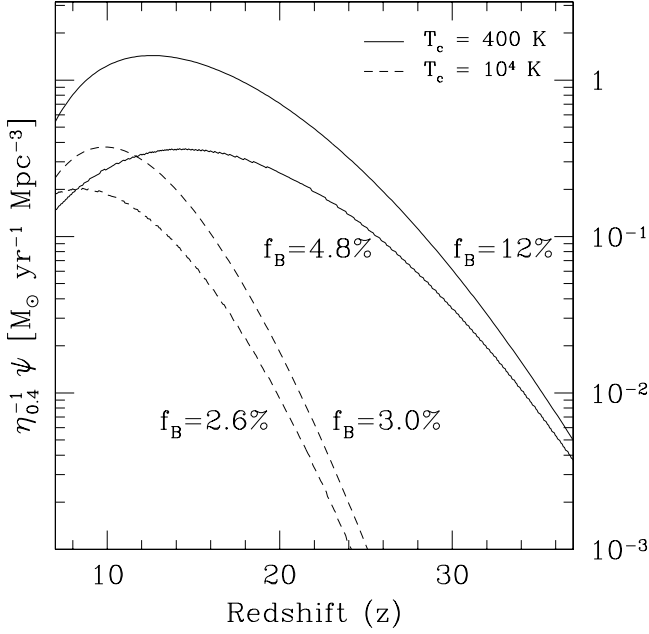


**Figure 1.** The star-formation rate (SFR) for the ongoing and single-burst models, for critical temperatures of  $T_c = 400$  (*solid lines*) and  $10^4$  K (*dashed lines*). For each  $T_c$  the upper curve is the ongoing SFR and the lower curve is the single-burst SFR. All curves are for  $\eta = 0.4$ ; each curve is labelled by the value of  $f_B \equiv \Omega_{\text{III}}(z=7)/\Omega_B$  it implies.

we simplify into the parameter  $\epsilon_{\text{pi}}$ ) and  $\Omega_{\text{III}}$ . For example, if  $\epsilon_{\text{pi}} = 1$  and  $f_B \equiv \Omega_{\text{III}}/\Omega_B \simeq 3 \times 10^{-3}$ , then Pop III stars would, in the mean, enrich the Universe to the solar abundance of silicon already at a redshift  $\gtrsim 7$ . In contrast, if  $\epsilon_{\text{pi}} = 0$ , then metallicity measurements place no constraints on the abundance of Pop III stars.

## 2.5 Star-formation model results

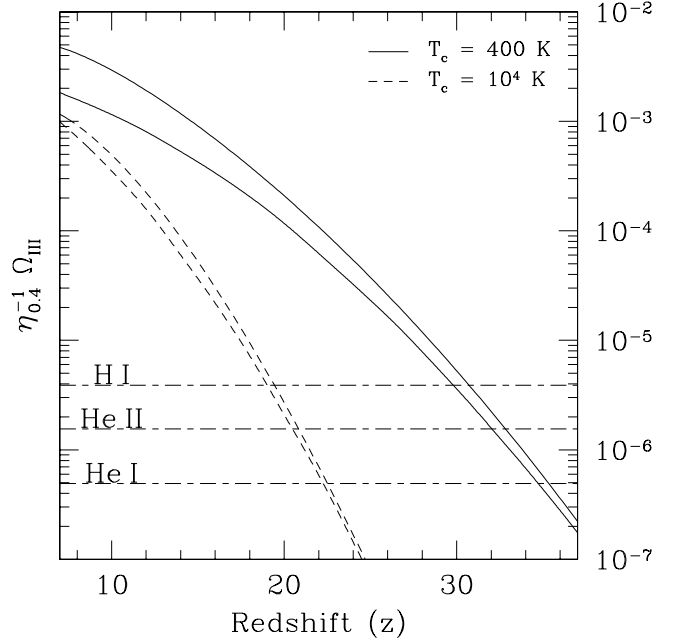
To compare our models, we present the SFR as a function of redshift in Fig. 1. We assume that Pop III star formation shuts off at  $z_{\text{end}} \simeq 7$ ; this may be due to photoevaporation of low-mass haloes due to reionization (Barkana & Loeb 1999) or some other process. Figure 1 shows the SFRs normalized to  $\eta = 0.4$ . The curves are labelled with the corresponding value of  $f_B$ .

Figure 2 shows  $\Omega_{\text{III}}(z)$  for the SFRs of Figure 1. The horizontal lines are explained in §5.

## 3 SPECTRA

### 3.1 Input stellar spectrum

Metal-free very massive stars have spectra similar to a  $\sim 10^5$  K blackbody spectrum (Bromm et al. 2001b). Most of the energy is then radiated in photons with energies  $> 13.6$  eV. There are also many photons produced capable of ionizing He II (but see Schaerer 2002). The specific luminosity per solar mass of very massive stars is almost independent of stellar mass (Bromm et al. 2001b). We will



**Figure 2.** The matter density processed through Pop III stars in units of the critical density, as a function of redshift. The four curves correspond to the four different SFRs of Fig. 1. The horizontal dashed lines labelled H I, He I and He II correspond to the  $\Omega_{\text{III}}$  required for Pop III stars to produce 10 ionizing photons per particle of each species. These lines are only relevant for the  $f_{\text{esc}} = 1$  case; see section 3.

therefore take the spectrum of a  $1000 M_{\odot}$  star as our fiducial input Pop III stellar spectrum.

When a Pop III star becomes luminous, we expect the host halo to contain gas not incorporated into stars; we call this gas the ‘nebula.’ We refer to the gas outside the collapsed halo as the IGM. The physical environment of Pop III star formation will likely undergo a transition from dense gas in the nebula to a diffuse IGM, but we will model all gas as either part of the nebula or part of the IGM. *We also assume that both the nebula and IGM are entirely free of dust.*

Since the nebula and IGM are neutral in the absence of stellar radiation, both have the potential to play an important role in reprocessing ionizing photons from a star. We examine two limiting cases for the importance of each of these phases: In the first case, Pop III stars are enshrouded in dense nebulae, and all of the reprocessing of ionizing radiation takes place in the halo (the IGM still plays a role in scattering Ly $\alpha$  photons). In this case, the escape fraction of ionizing photons from the nebula,  $f_{\text{esc}}$ , is zero. In the second case, the nebula plays no role and  $f_{\text{esc}} = 1$ ; all reprocessing occurs in the IGM. In the rest of this section, we discuss the reprocessed spectrum of Pop III stellar radiation for each of these cases.

### 3.2 No escape of ionizing radiation into the IGM

#### 3.2.1 Properties of a nebula

Numerical simulations suggest that when a Pop III star forms, the nebula consists of a higher density phase, with  $n_{\text{H}} \simeq 10^4 \text{ cm}^{-3}$ , and a lower density phase (e.g., Bromm et

al. 1999). We make the simplifying assumption that half of the nebula's mass is contained in a homogeneous phase with density  $n_{\text{H}} = 10^4 \text{ cm}^{-3}$  that completely covers the star(s), and ignore the lower density gas. We take the mass fractions of hydrogen and helium as  $X = 0.75$  and  $Y = 0.25$ , respectively.

Ionizing radiation from the star(s) creates an H II region in the dense nebula. Because of the hardness of our input spectrum, in the inner part of the H II region helium is doubly ionized (the He III region). In the outer part it is singly ionized (the He II region; the spectrum is hard enough that there is no H II/He I region). The majority of photons above the He II ionization threshold ionize He II rather than H I. We iteratively solve for the sizes and temperatures of these regions, using the thermodynamic equations from Cen (1992). The He III region, comprising 0.4 of the volume of the H II region, has a temperature of  $3.6 \times 10^4 \text{ K}$ ; the He II region is cooler, at  $2.7 \times 10^4 \text{ K}$ . In both regions the primary cooling mechanism is H I recombination, but free-free emission and cooling via collisional excitation of H I are also important. The total nebular emission is not very sensitive to the relative sizes of the He II and He III regions.

Given these properties of an ionized region, we can determine  $f_{\text{esc}}$ .<sup>†</sup> The volume and mass of the He III region are

$$V_{\text{HeIII}} = \frac{Q_{\text{HeII}}}{n_e n_{\text{HeIII}} \alpha_{\text{B}}(\text{He II}, T = 3.6 \times 10^4 \text{ K})}, \quad (9)$$

$$M_{\text{HeIII}} = \mu m_{\text{H}} (n_{\text{H}} + n_{\text{He}}) V_{\text{HeIII}} \simeq 0.7 \left( \frac{M_*}{M_{\odot}} \right), \quad (10)$$

where  $Q_{\text{HeII}}$  is the stellar emission rate of photons energetic enough to ionize He II,  $\alpha_{\text{B}}(\text{He II}, T)$  is the Case B recombination coefficient for He II, here  $M_*$  is the mass of the ionizing Pop III star(s) in the nebula and  $\mu = 1.2$  is the mean molecular weight. Because in the He III region recombinations to He II provide enough photons to keep the hydrogen ionized, the volume and mass of the He II region are

$$V_{\text{HeII}} = \frac{Q_{\text{HI}} - Q_{\text{HeII}}}{n_e n_{\text{HII}} \alpha_{\text{B}}(\text{H I}, T = 2.7 \times 10^4 \text{ K})}, \quad (11)$$

$$M_{\text{HeII}} = \mu m_{\text{H}} (n_{\text{H}} + n_{\text{He}}) V_{\text{HeII}} \simeq 1.0 \left( \frac{M_*}{M_{\odot}} \right), \quad (12)$$

where  $Q_{\text{HI}}$  is the rate of H I-ionizing photons, and  $\alpha_{\text{B}}(\text{H I}, T)$  is the hydrogen recombination coefficient.

The total mass of ionized gas is then 1.7 times the mass of the ionizing star(s). In the single-burst star-formation model, the nebula mass in  $n_{\text{H}} = 10^4 \text{ cm}^{-3}$  gas,  $M_{\text{neb}}$ , is

$$M_{\text{neb}} = \frac{1}{2} \frac{1 - \eta}{\eta} M_*. \quad (13)$$

For  $\eta = 0.4$ ,  $M_{\text{neb}} = 0.75 M_*$ , which implies  $f_{\text{esc}} = 0$  would be difficult to achieve for our model nebula. In the ongoing model, though,  $M_{\text{neb}} > (1 - \eta)M_*/(2\eta)$  in general, and especially at lower redshift. This is due to the short lifetime of Pop III stars: star formation in a halo subsequent to the first episode usually takes place after previous generations

<sup>†</sup> The dynamical evolution of the gas on the timescale of the lifetime of a Pop III star may be important, as the pressure of the nebular gas may exceed the gravitational pressure, but here we treat the nebula as static.

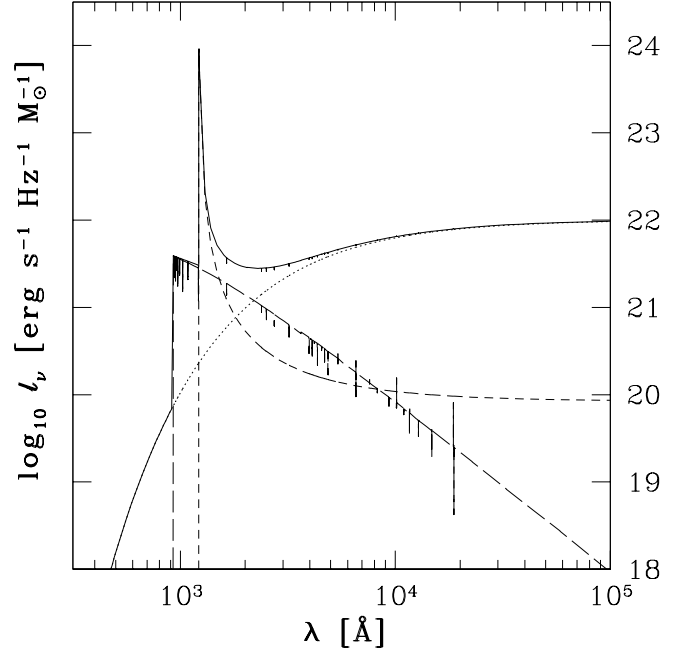


**Figure 3.** Spectrum of a  $z = 15$  Pop III star plus nebular emission, for the  $f_{\text{esc}} = 0$  case of section 3.2. The long-dashed line is the spectrum of the star, cut off for absorption shortward of the Lyman limit. The dotted line is the spectrum of free-free emission from the nebula. The short-dashed line is emission from Ly $\alpha$  recombination in the nebula at  $z = 15$ , corrected for scattering in the IGM. The solid line is the sum of the spectra. All spectra are in the rest frame of the star.

of stars in the halo have stopped radiating. Thus  $f_{\text{esc}} = 0$  may be possible in these haloes.

### 3.2.2 Resulting spectrum

**3.2.2.1 Recombination emission.** Approximately 1/2 of the energy radiated by a Pop III star in a nebula is ultimately reradiated by recombinations. The mean energy of a free electron just before it recombines with a proton may be estimated from

$$\langle E \rangle = \frac{\beta_{\text{B}}(\text{H I}, T) kT}{\alpha_{\text{B}}(\text{H I}, T)}, \quad (14)$$

where  $\beta_{\text{B}}(\text{H I}, T)$  is the recombination emission coefficient. Using  $T = 3 \times 10^4 \text{ K}$ , we find  $\langle E \rangle = 1.4 \text{ eV}$  (Seaton 1959; Cen 1992). The average energy radiated per recombination, then, is 15.0 eV. Under the on-the-spot approximation, all Lyman series photons degrade into  $n = 2 \rightarrow 1$  transitions, where  $n$  is the energy level of an excited hydrogen atom. Since 10.2 eV is released per  $n = 2 \rightarrow 1$  transition, about 2/3 of the recombination energy is released in Ly $\alpha$  or two-photon emission, and 1/3 of the recombination energy (and about 1/6 of the total emitted energy) is emitted in other recombination lines and free-bound continuous emission. We ignore those processes here; see Schaerer (2002) for a more complete computation of nebular emission lines and free-bound spectra.

The relative importance of Ly $\alpha$  emission compared to two-photon emission is determined by the effective recombination coefficients to the  $2p$  and  $2s$  states, respectively,

and the collisional excitation rate from the  $2s$  state to the  $2p$  state. At  $T = 3 \times 10^4$  K, 0.75 Ly $\alpha$  photons are emitted for every H I recombination (Osterbrock 1989; Storey & Hummer 1995); we ignore the contribution of two-photon emission (about 12 per cent of the total emission) to the spectrum.

Since Ly $\alpha$  photons resonantly scatter in neutral hydrogen, they will not travel far in the IGM until their frequencies are shifted away from the resonant frequency,  $\nu_{\text{Ly}\alpha}$ . Photons initially scattered blueward of the line resonance will eventually cosmologically redshift back into the resonance. The result is that the IGM ultimately scatters all Ly $\alpha$  photons to the red side of the line resonance (broadening from motions inside a halo doesn't contribute to the line profile). For a homogeneous, expanding IGM, the resulting scattered line profile,  $\phi(\nu, z)$ , was simulated by Loeb & Rybicki (1999), and we fit their result with

$$\phi(\nu, z) = \begin{cases} \nu_*(z) \nu^{-2} \exp\left[-\frac{\nu_*(z)}{\nu}\right] & \text{if } \nu > 0 \\ 0 & \text{if } \nu \leq 0 \end{cases}, \quad (15)$$

$$\nu_*(z) = 1.5 \times 10^{11} \text{ Hz} \left(\frac{\Omega_B h^2}{0.019}\right) \left(\frac{h}{0.7}\right)^{-1} \frac{(1+z)^3}{E(z)}. \quad (16)$$

This profile results in a strong, asymmetric Ly $\alpha$  emission line near 1220 – 1225 Å with a scattering tail extending to long wavelengths.

In the He III region, He II recombinations sometimes produce more than one photon capable of ionizing H I. Recombinations directly to the  $n = 2$  state produce He II Balmer continuum photons, which are capable of ionizing H I. In addition, two-photon decay from the  $2s$  state produces 1.42 H I-ionizing photons per decay (Osterbrock 1989). Since He II Ly $\alpha$  is also capable of ionizing hydrogen, the mean number of hydrogen ionizations per He II recombination is

$$\frac{\alpha_2(\text{He II}, T) + 1.42\alpha_{2s}^{\text{eff}}(\text{He II}, T) + \alpha_{2p}^{\text{eff}}(\text{He II}, T)}{\alpha_B(\text{He II}, T)} = 1.7, \quad (17)$$

where  $\alpha_2(\text{He II}, T)$  is the recombination coefficient for recombinations directly to the  $n = 2$  state and  $\alpha_{2l}^{\text{eff}}(\text{He II}, T)$  is the effective total recombination coefficient to the  $2l$  state (Storey & Hummer 1995).

**3.2.2.2 Free-free emission.** Free-free radiation accounts for about 1/4 of the cooling in the nebula. This energy is radiated in a continuous spectrum,

$$j_\nu^{\text{ff}} = 7.2 \times 10^{-39} \sum_Z n_e n_Z Z^2 \left(\frac{T}{\text{K}}\right)^{-1/2} \times \exp\left(\frac{-h\nu}{kT}\right) \text{ erg s}^{-1} \text{ cm}^3 \text{ Hz}^{-1} \text{ ster}^{-1}, \quad (18)$$

where  $j_\nu^{\text{ff}}$  is the specific emission coefficient,  $\nu$  is the frequency of emitted radiation and  $n_Z$  is the number density of ions of net charge  $Z$  (Ferland 1980). A Gaunt factor of 1.3 has been assumed; this results in an error of less than 8 per cent over optical and UV frequencies (Karzas & Latter 1961).

The luminosity per solar mass of Pop III stars from free-free radiation,  $l_\nu^{\text{ff}}$ , is

$$l_\nu^{\text{ff}} = \frac{4\pi}{M_*} \left( j_\nu^{\text{ff, He III}} V_{\text{He III}} + j_\nu^{\text{ff, He II}} V_{\text{He II}} \right). \quad (19)$$

Here He III and He II label the emission coefficients and volumes computed for the He III and He II *regions*; in each case the free-free emission is dominated by H II.

### 3.2.2.3 Emission from collisional excitation of H I.

Collisions between a free electron and trace H I atom sometimes excite the H I atom, which then radiates away the excitation energy. The collisional excitation rate coefficient for transitions from the  $n = 1$  state to state  $u$ ,  $q_{1u}$ , is

$$q_{1u} = \frac{8.629 \times 10^{-6}}{T^{1/2}} \frac{\Omega(1, u)}{\omega_1} \exp\left(\frac{-\chi(1, u)}{kT}\right) \text{ s}^{-1} \text{ cm}^3, \quad (20)$$

where  $T$  is in K,  $\Omega(1, u)$  is the (temperature-dependent) effective collision strength for transitions from the  $n = 1$  to state  $u$ ,  $\omega_1$  is the statistical weight of the  $n = 1$  state and  $\chi(1, u)$  is the energy difference between the  $n = 1$  and state  $u$  (Osterbrock 1989).

We compute the collisional excitation to the  $n = 2$  and  $n = 3$  states using cross-sections from Callaway (1985) and Callaway, Unnikrishnan & Oza (1987). These excitations result in additional Ly $\alpha$  emission: excitations to the  $2p$ ,  $3s$  and  $3d$  states radiatively decay to  $n = 1$  via Ly $\alpha$  photons, and atoms in the  $2s$  state (resulting from collisions to either the  $2s$  or  $3p$  state) may be additionally collisionally excited to the  $2p$  state. The rate of collisional Ly $\alpha$  emission per unit stellar mass,  $q_{\text{Ly}\alpha}^{\text{coll}}$ , is

$$q_{\text{Ly}\alpha}^{\text{coll}} = n_e n_{\text{HI}} q_{1,2p}^{\text{eff}} \left(\frac{V}{M_*}\right), \quad (21)$$

where

$$q_{1,2p}^{\text{eff}} = \sum_u L(u) q_{1u} \quad (22)$$

and

$$L(u) = \begin{cases} 1 & \text{if } u \in (2p, 3s, 3d) \\ 0.33 & \text{if } u \in (2s, 3p) \end{cases}. \quad (23)$$

The factor of 0.33 accounts for  $2s$  to  $2p$  collisional excitation (Osterbrock 1989). Summing over the He II and He III regions,  $q_{\text{Ly}\alpha}^{\text{coll}} = 3.4 \times 10^{47} \text{ s}^{-1} M_\odot^{-1}$ .

**3.2.2.4 Total spectrum.** For the  $f_{\text{esc}} = 0$  case, the total specific luminosity per unit stellar mass emitted from a Pop III star and nebula and scattered in the IGM,  $l_\nu^0(z)$ , has three components that we treat: the truncated stellar spectrum,  $l_\nu^{*a}$ , the free-free spectrum,  $l_\nu^{\text{ff}}$ , and the scattered Ly $\alpha$  spectrum,  $l_\nu^{\text{Ly}\alpha}(z)$ :

$$l_\nu^0(z) = l_\nu^{*a} + l_\nu^{\text{ff}} + l_\nu^{\text{Ly}\alpha}(z). \quad (24)$$

The truncated stellar spectrum is

$$l_\nu^{*a} = \begin{cases} l_\nu^* & \text{if } h\nu < 13.6 \text{ eV} \\ 0 & \text{if } h\nu \geq 13.6 \text{ eV} \end{cases}. \quad (25)$$

The  $l_\nu^{*a}$  spectrum is slightly modified between 912 and 1216 Å by scattering in the IGM, when the photons in that range are cosmologically redshifted into the Ly $\alpha$  resonance (e.g., Peebles 1993). This effect is small when  $1.75 \nu_*(z) \ll 8.22 \times 10^{14} \text{ Hz}$ , i.e., the width of the scattered Ly $\alpha$  line (Loeb & Rybicki 1999) is small compared to the frequency difference between 912 Å and 1216 Å. Since  $1.75 \nu_*(z = 30) = 8.27 \times 10^{13} \text{ Hz}$ , we ignore this correction to the spectrum.

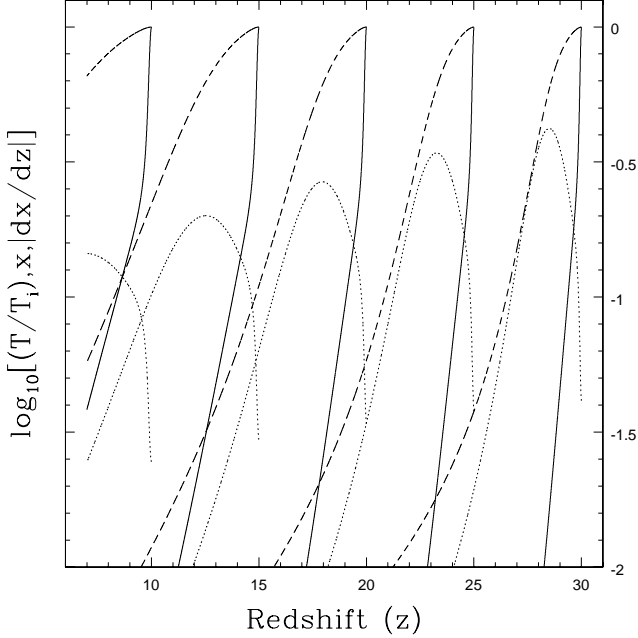


**Figure 4.** Properties of the ionized IGM near a Pop III star. There are sets of three curves for five values of  $z_i = (10, 15, 20, 25, 30)$ . In each set of curves, the solid line is the temperature as a fraction of the initial temperature, the dashed line is the ionization fraction and the dotted line is  $|dx/dz|$ , followed from  $z_i$  to  $z = 7$ .

The free-free spectrum is given by eq. (19). The Ly $\alpha$  spectrum is

$$l_{\nu}^{\text{Ly}\alpha}(z) = q_{\text{Ly}\alpha} h\nu_{\text{Ly}\alpha} \phi(\nu_{\text{Ly}\alpha} - \nu, z), \quad (26)$$

where  $q_{\text{Ly}\alpha}$  is the rate of Ly $\alpha$  photons produced per solar mass of the ionizing star. That rate is

$$q_{\text{Ly}\alpha} = 0.75 (q_{\text{HI}} - q_{\text{HeII}} + 1.7 q_{\text{HeII}}) + q_{\text{Ly}\alpha}^{\text{coll}}, \quad (27)$$

where  $q_{\text{HI}} \equiv Q_{\text{HI}}/M_*$  and  $q_{\text{HeII}} \equiv Q_{\text{HeII}}/M_*$ . The factor 0.75 represents the fraction of hydrogen recombinations that result in Ly $\alpha$  photons, and the factor of 1.7 accounts for the number of hydrogen ionization per HeII recombination, computed above.

Figure 3 show  $l_{\nu}^{*a}$ ,  $l_{\nu}^{\text{ff}}$ ,  $l_{\nu}^{\text{Ly}\alpha}(z)$  and  $l_{\nu}^0(z)$  for  $z = 15$ . In this model no Pop III ionizing photons escape to the IGM, thus Pop III stars don't contribute to reionization of the Universe (cf. section 3.3).

### 3.3 Complete escape of ionizing radiation into the IGM

#### 3.3.1 Properties of the IGM

The second case we consider is that the nebula plays no role in reprocessing ionizing radiation from a Pop III star,  $f_{\text{esc}} = 1$ . This may be because, in contrast to the assumptions we made in §3.2.1, the density of the nebula is low, or because the nebula is clumped into high-density regions with a small covering fraction, or because the nebula was blown away by the star(s). Because the timescales of important IGM processes extend beyond the lifetime of a Pop III star, in this

section we will name the redshift of formation of a Pop III star  $z_i$ , and then describe the evolution as a function of  $z$ .

We assume the IGM is uniform with baryon density  $n_{\text{IGM}}(z) = 1.7 \times 10^{-7} (1+z)^3 \text{ cm}^{-3}$  (which ignores the small fraction of baryons in collapsed haloes),  $X = 0.75$  and  $Y = 0.25$ . Ionizing photons from a Pop III star stream into the IGM and form an ionized region. Because the density is low, for  $z_i \lesssim 30$  recombinations are of little importance on the timescale of the star's lifetime,  $\tau \simeq 2 \times 10^6 \text{ yr}$ . For the purposes of calculating the properties of the ionized region of the IGM, we assume that all of the ionizations occur immediately; at worst this contributes less than a 3 per cent error to the computed spectrum.

HeIII recombines more quickly than HII, and HeI recombinations occur on a comparable timescale to those of HI. As discussed in §3.2.2.1, HeII recombinations produce 1.7 H I-ionizing photons on average. In the low-density limit, a HeI recombination ionizes 1 hydrogen atom (Osterbrock 1989). We treat HeI and HeII ionizations as an extra 1 and 1.7 H I ionizations, respectively, and track only hydrogen recombinations.

For  $z_i \lesssim 30$ , a Pop III star ionizes a volume of the IGM,  $V(z)$ , initially given by

$$V(z_i) = \frac{(Q_{\text{HI}} + 0.7 Q_{\text{HeII}}) \tau}{n_{\text{IGM}}(z)} = \frac{2.4 \times 10^4}{(1+z_i)^3} \left( \frac{M_*}{M_{\odot}} \right) \text{ kpc}^3. \quad (28)$$

The initial temperature in this volume is determined from photoionization heating to be  $T_i \simeq 6 \times 10^4 \text{ K}$ . Given  $z_i$ , we solve the temperature evolution of the ionized IGM region as a function of  $z$  until  $z = 7$ , when we assume that the Universe reionizes. If Pop III stars reionize the Universe before  $z = 7$ , their ionized nebulae will have overlapped, and the analysis of this section will no longer be appropriate. The post-reionization contribution of the IGM to the CIRB depends on the temperature and ionization state of the IGM, but is expected to be small under typical assumptions. But the most important effect that reionization would have on the Pop III contribution the CIRB may be the effect reionization has on the SFR. As noted in §2.5, reionization may stop or severely curtail the formation of Pop III stars.

To compute the temperature of the ionized IGM around a Pop III star as a function of redshift, we set the initial temperature to  $T_i = 6 \times 10^4 \text{ K}$  and follow the evolution of temperature considering cooling from Compton scattering of CMBR photons off of electrons, adiabatic cooling of the IGM from the expansion of the Universe, cooling from collisional excitation of H I, free-free cooling and recombination cooling (Cen 1992). Since all of those processes except adiabatic cooling depend on the ionization fraction,  $x$ , it is solved for simultaneously, using the approximation  $x \simeq n_e/n_{\text{IGM}}$ :

$$-\frac{dx}{dt} = \alpha_{\text{B}}(\text{HI}, T) n_{\text{IGM}} x^2 \quad (29)$$

(e.g., Peebles 1993). Figure 4 plots  $T(z)$ ,  $x(z)$  and  $|dx(z)/dz|$  for five values of  $z_i$ .

Initially nearly all the hydrogen is ionized, and Compton cooling briefly dominates the thermodynamics. Once a small fraction,  $\sim 10^{-4}$ , of the hydrogen atoms have recombined, cooling via collisional excitation becomes the dominant process. As the temperature decreases, the recombination rate increases, which in turn increases the neutral fraction and thus the collisional cooling rate. When the tempera-

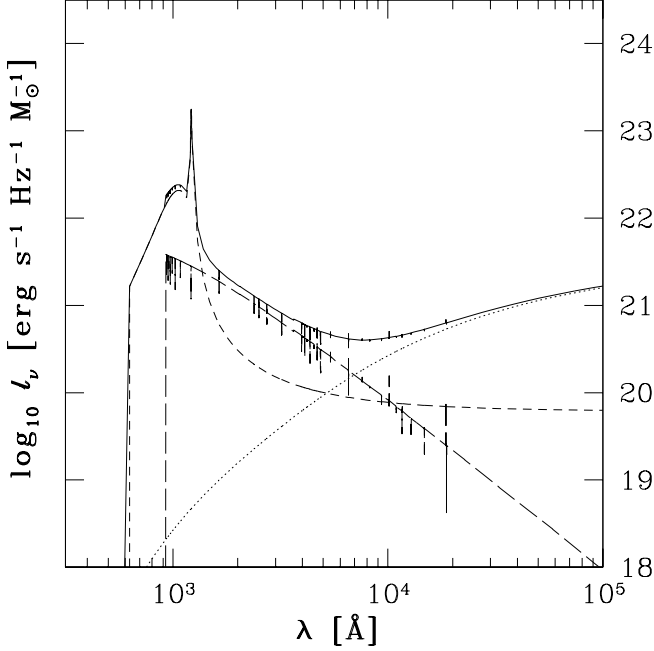


**Figure 5.** Spectrum of a  $z = 15$  Pop III star plus emission from the IGM, for the  $f_{\text{esc}} = 1$  case of section 3.3. The long-dashed line is the spectrum of the star, cut off for absorption shortward of the Lyman limit. The dotted line is the spectrum of free-free emission from the IGM. The short-dashed line is emission from Ly $\alpha$  recombination in the IGM, corrected for scattering. The free-free and Ly $\alpha$  spectra are integrated from  $z = 15$  to  $z = 7$ , and divided by the lifetime of a Pop III star to give a useful normalization. The solid line is the sum of the spectra. The sharp peak at 1216 Å is collisionally excited Ly $\alpha$  emission; the broad peak at 1000 Å is Ly $\alpha$  from recombinations. All spectra are in the rest frame of the star (see Section 3.3.2 for explanation).

ture reaches about  $1.5 \times 10^4$  K, Compton cooling dominates again. For lower values of  $z_i$ , adiabatic cooling eventually dominates; for higher values of  $z_i$ , recombination cooling becomes important. Free-free emission is important enough to be included.

### 3.3.2 Resulting spectrum

**3.3.2.1 Recombination emission.** As in §3.2.2.1, we consider only the Ly $\alpha$  component of the recombination spectrum. The rate of production of Ly $\alpha$  photons from recombinations,  $q_{\text{Ly}\alpha}^{\text{rec}}$ , is

$$q_{\text{Ly}\alpha}^{\text{rec}} = 0.63 (q_{\text{HI}} - q_{\text{HeII}} + 1.7 q_{\text{HeI}}) \tau \left| \frac{dx}{dt} \right|, \quad (30)$$

where 0.63 is a representative value for the fraction of hydrogen recombinations resulting in Ly $\alpha$  emission near the peak of the recombination rate.

**3.3.2.2 Free-free emission.** The free-free spectrum is

$$j_{\nu}^{\text{ff}} = 7.2 \times 10^{-39} x^2 n_{\text{IGM}}^2 \left( \frac{T}{\text{K}} \right)^{-1/2} \times \exp \left( \frac{-h\nu}{kT} \right) \text{erg s}^{-1} \text{cm}^3 \text{Hz}^{-1} \text{ster}^{-1} \quad (31)$$

(Ferland 1980). The specific luminosity per unit stellar mass is

$$l_{\nu}^{\text{ff}}(z, z_i) = 4\pi j_{\nu}^{\text{ff}} \frac{V(z)}{M_*} = 1.6 \times 10^{18} x^2 (1+z)^3 \left( \frac{T}{\text{K}} \right)^{-1/2} \times \exp \left( \frac{-h\nu}{kT} \right) \text{erg s}^{-1} \text{Hz}^{-1} \text{M}_{\odot}^{-1}, \quad (32)$$

where the second equality follows from equation (28). The  $z_i$  dependence of  $l_{\nu}^{\text{ff}}$  results from the implicit dependence of  $T$  and  $x$  on  $z_i$  and  $z$ .

### 3.3.2.3 Emission from collisional excitation of H I.

The rate of Ly $\alpha$  photons produced by collisional excitations is given by eqs. (21) and (28):

$$q_{\text{Ly}\alpha}^{\text{coll}} = 2.0 \times 10^{55} x(1-x)(1+z)^3 q_{1,2p}^{\text{eff}} \text{cm}^{-3} \text{M}_{\odot}^{-1}. \quad (33)$$

In the low density limit, though, collisions from the  $2s$  to  $2p$  state are unimportant, so

$$L(u) = \begin{cases} 1 & \text{if } u \in (2p, 3s, 3d) \\ 0 & \text{if } u \in (2s, 3p) \end{cases}. \quad (34)$$

Additionally, because the temperature in the IGM varies, we make the following fits to the data of Callaway et al. (1987):

$$\Omega(1, 2p) \simeq -2.41 \times 10^{-3} \left( \frac{T}{10^4} \right)^2 + 0.148 \left( \frac{T}{10^4} \right) + 0.170 \quad (35)$$

and

$$\begin{aligned} &\Omega(1, 3s) + \Omega(1, 3d) \\ &\simeq -2.29 \times 10^{-3} \left( \frac{T}{10^4} \right)^2 + 0.0299 \left( \frac{T}{10^4} \right) + 0.116. \quad (36) \end{aligned}$$

The fits are good to better than 5 per cent for temperatures from  $1.6 \times 10^4$  to  $6 \times 10^4$  K, where almost all of the collisional excitation occurs.

**3.3.2.4 Total spectrum.** For the  $f_{\text{esc}} = 1$  case, the total specific luminosity per unit stellar mass emitted from a Pop III star and IGM, including scattering, is  $l_{\nu}^0(z)$ . We treat the same three components as in the  $f_{\text{esc}} = 0$  case: the truncated stellar spectrum,  $l_{\nu}^{*a}$ , the free-free spectrum,  $l_{\nu}^{\text{ff}}(\nu, z, z_i)$ , and the scattered Ly $\alpha$  spectrum,  $l_{\nu}^{\text{Ly}\alpha}(\nu, z, z_i)$ . The truncated stellar spectrum is given by eq. (25), and the free-free spectrum is given by eq. (32). Similar to eq. (26), the Ly $\alpha$  spectrum is

$$l_{\nu}^{\text{Ly}\alpha}(z, z_i) = q_{\text{Ly}\alpha} h\nu_{\text{Ly}\alpha} \phi(\nu_{\text{Ly}\alpha} - \nu, z), \quad (37)$$

where

$$q_{\text{Ly}\alpha}(z, z_i) = q_{\text{Ly}\alpha}^{\text{rec}} + q_{\text{Ly}\alpha}^{\text{coll}}. \quad (38)$$

The total spectrum emitted by a Pop III star and the surrounding IGM from the formation of the star at  $z_i$  to the redshift at which the Universe is reionized,  $z = z_{\text{reion}}$ , expressed in the rest frame of the star when it forms and normalized to the lifetime of the star, is

$$l_{\nu}^1(\nu, z_i) = l_{\nu}^{*a}(\nu) + \frac{1}{\tau} \int_{z_{\text{reion}}}^{z_i} dz \left| \frac{dt}{dz} \right| [l_{\nu}^{\text{ff}}(\nu', z, z_i) + l_{\nu}^{\text{Ly}\alpha}(\nu', z, z_i)], \quad (39)$$

with

$$\nu' = \nu \left( \frac{1+z}{1+z_i} \right). \quad (40)$$

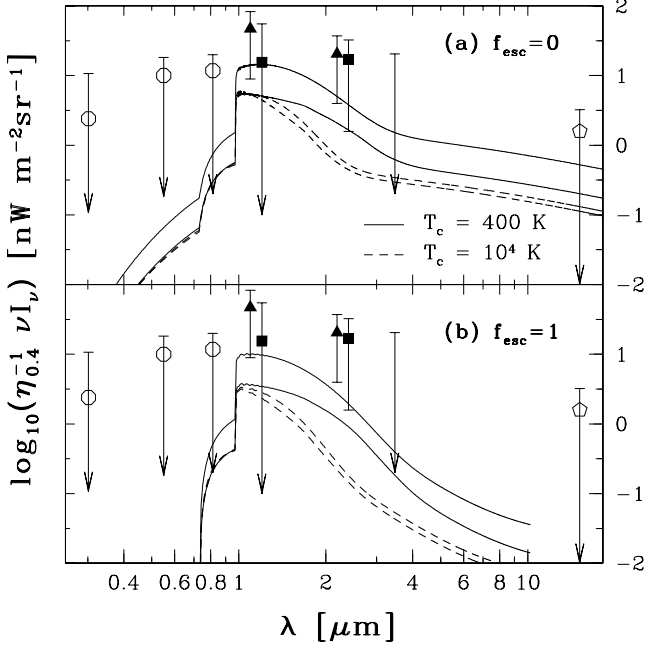


**Figure 6.** The cosmic infrared background from Pop III stars. The ordinate is observed frequency multiplied by observed specific intensity. Shown are curves for star formation in haloes with virial temperatures above critical temperatures  $T_{\text{crit}} = 400$  K (molecular-hydrogen cooling, solid lines) and  $10^4$  K (atomic-hydrogen cooling, dashed lines). (a)  $f_{\text{esc}} = 0$ . (b)  $f_{\text{esc}} = 1$ . For both  $f_{\text{esc}}$  cases, there are two sets of two curves: the upper set is for the ongoing star-formation model; the lower set is for the single-burst model. The properties of the curves are explained in §4.1; this figure shows  $z_{\text{end}} = 7$ . The points show the excess CIRB, with  $2\sigma$  errors, and are described in §4.2.

Because this spectrum is in the frame of the star when it forms, IGM emission at later times (and thus lower values of  $z$ ) appears in the spectrum at *higher* frequencies than it is emitted at; this is because we *blueshift* all of the IGM radiation back to redshift  $z_i$ . The spectra are normalized by integrating the emission from  $z_i$  to  $z = 7$  and dividing by the lifetime of the star,  $\tau$ . The resulting spectrum isn't meaningful for the observation of a single Pop III stellar source plus ionized IGM region, because the photons are emitted at different times, but it is a useful spectrum for computing the CIRB. The spectrum of a single source at redshift  $z < z_i$  (such that the star no longer contributes directly to the spectrum) is

$$l_\nu^1(\nu, z, z_i) = l_\nu^{\text{ff}}(\nu, z, z_i) + l_\nu^{\text{Ly}\alpha}(\nu, z, z_i); \quad (41)$$

this spectrum is in the frame of the emission at redshift  $z$ .

Figure 5 shows  $l_\nu^{*a}$ ,  $l_\nu^{\text{ff}}(z_i)$ ,  $l_\nu^{\text{Ly}\alpha}(z_i)$  and  $l_\nu^1(z_i)$  for  $z_i = 15$ . The sharp emission peak at  $1216 \text{ \AA}$  results from collisionally-excited Ly $\alpha$  emission shortly after the star forms. The broad peak centered near  $1000 \text{ \AA}$  is Ly $\alpha$  emission from recombinations. At  $608 \text{ \AA}$  the Ly $\alpha$  spectrum is cut off as a consequence of integrating the IGM spectrum to  $z = 7$ ; the cut-off location is  $1216 \text{ \AA} (1 + z_{\text{reion}})/(1 + z_i)$ .

## 4 COSMIC INFRARED BACKGROUND

### 4.1 Model results

We now convolve the processed spectra of Section 3 with the star-formation histories of Section 2 to calculate the Pop III contribution to the CIRB. The background is evaluated with

$$\nu_{\text{obs}} I_\nu = c \int_0^\infty dz \left| \frac{dt}{dz} \right| \frac{\nu(z) j_\nu^c(z)}{1+z} \quad (42)$$

(e.g., Peebles 1993). Here  $\nu_{\text{obs}}$  is the observed frequency,  $I_\nu$  is the observed specific intensity,  $\nu(z) = (1+z)\nu_{\text{obs}}$  and  $j_\nu^c(z)$  is the comoving specific emission coefficient. Both the star-formation history and the assumed recombination history determine  $j_\nu^c(z)$ :

$$j_\nu^c(z) = \frac{1}{4\pi} l_\nu \tau \psi(z), \quad (43)$$

where  $l_\nu$  is either  $l_\nu^0$  or  $l_\nu^1$ ,  $\tau = 2 \times 10^6$  yr is the fiducial main-sequence lifetime of a Pop III star (Bromm et al. 2001b) and  $\psi(z)$  is either  $\psi_{\text{on}}(z)$  or  $\psi_{\text{burst}}(z)$ , the SFR per comoving volume.

Results for  $f_{\text{esc}} = 0$  and 1 are shown in Fig. 6. There are a total of eight curves in the figure, generated by varying each of three parameters over two values:  $f_{\text{esc}} = 0$  or 1;  $T_{\text{crit}} = 400$  or  $10^4$  K; star-formation mode of ongoing or single-burst. Models with  $f_{\text{esc}} = 0$  always produce more CIRB at all wavelengths than  $f_{\text{esc}} = 1$  models. Models with  $T_{\text{crit}} = 400$  K produce more CIRB than  $T_{\text{crit}} = 10^4$  K models at all wavelengths except near  $1 \mu\text{m}$  for single-burst star-formation models. The ongoing star-formation models produce more CIRB at all wavelengths than single-burst star-formation models, except near  $1 \mu\text{m}$  for the  $f_{\text{esc}} = 0$  case.

The sharp edge at  $1 \mu\text{m}$  in all of the curves is a result of our sharp truncation of Pop III star formation at  $z_{\text{end}} = 7$ . The edge occurs at the redshifted wavelength of Ly $\alpha$  from stars at  $z_{\text{end}}$ , i.e.,  $(1 + z_{\text{end}})1216 \text{ \AA}$ . The reason that the CIRB curves for  $T_{\text{crit}} = 400$  and  $10^4$  K have similar values at  $1 \mu\text{m}$  for single-burst star-formation models is that the corresponding SFRs at  $z = 7$  are similar (see Fig. 1).

The ‘‘bump’’ in the CIRB curves from  $0.7 \mu\text{m}$  to  $1 \mu\text{m}$  results from stellar emission between rest-frame  $912$  and  $1216 \text{ \AA}$  (see Figs. 3 and 5) by sources at  $z = 7$ . From  $\lambda = 1 \mu\text{m}$  to roughly  $2 \mu\text{m}$  the Pop III CIRB is dominated by Ly $\alpha$  emission from sources at  $1 + z = \lambda/1216 \text{ \AA}$ . The inflection points of the curves, particularly clear in the  $f_{\text{esc}} = 0$  panel, occur at the wavelength where the Pop III CIRB transitions from being dominated by Ly $\alpha$  emission to being dominated by continuum emission from sources at  $z = z_{\text{end}}$ . The continuum radiation for the  $f_{\text{esc}} = 0$  spectrum is dominated by free-free emission (see Fig. 3), whereas stellar continuum is important as well for the  $f_{\text{esc}} = 1$  continuum spectrum (see Fig. 5). Consequently, the Pop III mid-IR background is determined predominantly by the choice of  $z_{\text{end}}$  rather than the SFR at extremely high redshifts. The Pop III contribution to the optical background (for  $z_{\text{end}} \geq 7$ ) is due to the stellar ‘‘bump’’ described above and the high-energy tail of free-free emission, which is only significant for the  $f_{\text{esc}} = 0$  spectrum; this is a consequence of the temperature of the gas, which is effectively much higher in the  $f_{\text{esc}} = 0$  case than for the  $f_{\text{esc}} = 1$  case (see §3).

## 4.2 Observational data

The points with error bars in Fig. 6 show the difference between the total extragalactic background and the extragalactic background due to resolved sources. At wavelengths, e.g.,  $0.3 \mu\text{m}$ , where the lower limit is an arrow, the contribution from resolved sources is sufficient to explain *all* of the background, at the  $2\sigma$  level. At wavelengths where data points have lower limits plotted, e.g.,  $2.2 \mu\text{m}$ , the light from resolved sources is not enough to account for the measured background. It is this unexplained excess, measured by Cambr esy et al. (2001) at  $1.25 \mu\text{m}$  and by Cambr esy et al. (2001) and Wright & Johnson (2001) at  $2.2 \mu\text{m}$ , that we are trying to fit with our models, while conforming to upper limits at other wavelengths.

**Near-IR data points** The triangles at  $1.25$  and  $2.2 \mu\text{m}$  ( $J$  and  $K$  band, respectively) correspond to the unexplained CIRB as measured by Cambr esy et al. (2001): they measured the total extragalactic background with *COBE*/DIRBE data, and subtracted from that the contribution due to resolved galaxies measured by near-IR surveys. The squares at  $J$  and  $K$  (offset slightly in wavelength for clarity) are our computation of the unexplained CIRB from the CIRB measurement of Wright & Johnson (2001), using their measurement of the total extragalactic background from *COBE*/DIRBE data (but using a different foreground model from Cambr esy et al. 2001), and the same galaxy contribution subtraction and error propagation as Cambr esy et al. (2001). The Wright & Johnson (2001) point at  $J$  band is consistent at the  $2\sigma$  level with no unexplained extragalactic background. All error bars are  $2\sigma$ . The  $2\sigma$  upper limit at  $3.5 \mu\text{m}$  ( $L$  band) represents a measurement of the total extragalactic background at that wavelength (Wright & Johnson 2001). *SIRTF* is expected to accurately measure the contribution of galaxies to the  $L$ -band CIRB, and thus allow a determination of the excess  $L$ -band CIRB (W. T. Reach, private communication).

**Other data points** The upper limits at  $0.3$ ,  $0.6$ , and  $0.8 \mu\text{m}$  are  $2\sigma$  upper limits on the unexplained optical extragalactic background light (Bernstein, Freedman, & Madore 2002). The open circle data points show the estimated unexplained optical extragalactic background, which is consistent with zero ( $2\sigma$ ) at all three bandpasses. Bernstein et al. (2002) measured the total optical extragalactic background from *HST* images (utilising simultaneous ground-based spectra for absolute zodiacal-light subtraction calibration). From published number counts and their own careful photometry of the Hubble Deep Field observations, they find no evidence for convergence in the integrated light from galaxies; this suggests that deeper galaxy photometry will lower the upper limits.

The upper limit at  $15 \mu\text{m}$  is our computation of the  $2\sigma$  upper limit on the unexplained mid-IR background light, using the CIRB upper limits obtained by Renault et al. (2001) from gamma-ray observations, and the *ISO*/*ISOCAM*  $15 \mu\text{m}$  galaxy counts reported by Elbaz et al. (2002). The open hexagonal data point shows the estimated excess CIRB, which is consistent with zero ( $2\sigma$ ).

## 5 DISCUSSION

Our models identify a very narrow range of parameter space in which Pop III stars may explain the excess CIRB:

(i) The Pop III stars must be very massive, so that most of their energy is radiated in photons energetic enough to ionize hydrogen.

(ii) Cooling in low-mass haloes is possible due to  $\text{H}_2$ .

(iii) Approximately 40 per cent of the eligible baryons in the star forming halo must be converted into Pop III stars.

(iv) The escape fraction of ionizing photons from the nebula surrounding a Pop III star must be near zero, so that most of the ionizing photons are converted into  $\text{Ly}\alpha$  photons.

(v) Pop III star formation must begin by  $z \simeq 25$  and persist until  $z_{\text{end}} \simeq 7$ , so that the  $\text{Ly}\alpha$  emission (Fig. 6) extends through the observed  $J$  and  $K$  bands.

(vi) Negative feedback effects must not inhibit Pop III star formation. In particular, we require that Pop III stars do not radiatively or mechanically destroy star-forming material, and that they do not enrich their surroundings with a sufficient amount of metals to end Pop III star formation.

The amplitudes of the curves in Fig. 6 scale simply with  $\eta$ , and they do not change dramatically with small changes to the cosmological parameters. The characteristic breaks in the spectra are located at  $912 \text{ \AA}(1 + z_{\text{end}})$  and  $1216 \text{ \AA}(1 + z_{\text{end}})$ , where  $z_{\text{end}}$  is the low-redshift limit to Pop III star formation; if  $z_{\text{end}}$  were much higher than 7, the Pop III CIRB peak would lie longward of the  $J$  band.

If all of the above conditions are met, then *all* of the observed near-IR CIRB deficit is due to Pop III star formation. Future observations may demonstrate that other sources contribute significantly to the near-IR background; e.g., part of the deficit could be due to the faint wings of galaxies that are unaccounted for in current surveys (Totani et al. 2001). The parameter space explored in this paper easily accommodates lower values of the unexplained CIRB, through decreasing the efficiency,  $\eta$ . The shape of the Pop III CIRB spectrum in the near-IR is primarily determined by the shape of the star-formation rate as a function of redshift.

The formation of very massive stars probably requires that the star-forming gas is not enriched with heavy elements to a mass fraction  $Z_{\text{crit}} \gtrsim 10^{-3} Z_{\odot}$ , where  $Z_{\odot}$  is the solar value (Bromm et al. 2001a). We require a large fraction of the mass processed through Pop III stars to end up in massive black holes, so as not to overproduce metals compared to the observed levels in the high redshift IGM and to avoid enriching the primordial gas too quickly to  $Z_{\text{crit}}$ . Recently, Schneider et al. (2002) have pointed out the possible problem that if *all* Pop III stars collapsed into massive black holes, the IGM would always have zero metallicity. It seems natural to assume, however, that a small fraction of the Pop III stellar mass,  $\Omega_Z = Z\Omega_B = \epsilon_{\text{pi}}\Omega_{\text{III}}$  is ejected into the IGM through pair-instability supernovae, even if the majority of the mass is permanently locked up in black holes. Assuming a ratio  $\Omega_{\text{III}}/\Omega_B \sim 0.1$ , the required pair-instability fraction to produce the critical level of metallicity  $Z_{\text{crit}}$  would be  $\epsilon_{\text{pi}} \sim 10^{-2}$  (see also Oh et al. 2001).

We thus conclude that if Pop III stars explain a large fraction of the near-IR background, then almost all Pop III

material must end up in massive black holes. In that case we would predict a significant contribution,  $\sim 10$  per cent, by massive black holes to the total baryonic mass budget in the Universe. Although such a prediction may seem somewhat extreme, it will ultimately be tested by observations (e.g., Agol & Kamionkowski 2001; Schneider et al. 2002). We emphasize that at present there are no observations that rule out such a scenario (e.g., Carr 1994). Moreover, there are good physical reasons to seriously consider the existence of massive black holes resulting from Pop III star formation (e.g., Bromm et al. 2002; Madau & Rees 2001; Schneider et al. 2002).

In §2.4 we discussed  $\Omega_{\text{III}}$ , the cumulative matter density processed through Pop III stars. In Fig. 2 the horizontal lines labelled H I, He I and He II correspond to the  $\Omega_{\text{III}}$  required to produce 10 ionizing photons per particle of each species (Bromm et al. 2001b). For the  $f_{\text{esc}} = 1$  model, the intersection of those lines with the  $\Omega_{\text{III}}$  star curves is expected to be closely related to the redshift of reionization. For the  $f_{\text{esc}} = 0$  model, though, Pop III ionizing photons are all absorbed in the haloes in which they are emitted, and thus Pop III stars make no contribution to the reionization of the Universe. We discussed above that if Pop III stars enriched their immediate environment with a sufficient amount of metals, Pop III stars would no longer form there (producing a SFR similar to our single-burst model). If metals from Pop III stars efficiently mixed throughout the Universe, the era of Pop III stars might therefore come to an end (see Bromm et al. 2001a).

A single Pop III star produces  $\sim 10^{37}$  erg s $^{-1}$  M $_{\odot}^{-1}$  in the Ly $\alpha$  line, assuming  $f_{\text{esc}} = 0$ . At  $z = 7$  that would result in a flux of  $\sim 10^{-23}$  erg s $^{-1}$  cm $^{-2}$  M $_{\odot}^{-1}$ . For a discussion of the size of the Ly $\alpha$  emitting region, see Loeb & Rybicki (1999). For the  $f_{\text{esc}} = 1$  case the luminosity and size of the emitting region of a Pop III star depend in more detail on redshift and IGM parameters.

Future theoretical work should improve our understanding of the efficiency of Pop III star formation, as well as the physical conditions of the haloes in which Pop III stars form. We finally expect the launch of *NGST* to open an observational window into the earliest epochs of star formation, possibly including Pop III stars, less than a decade from now.

## ACKNOWLEDGMENTS

VB thanks the TAPIR group at Caltech for its hospitality during the completion of this work. We thank L. Cambr esy, W. T. Reach, Y. Lithwick, A. Benson, J. Silk, A. Ferrara, M. Rees and P. Natarajan for stimulating discussions. We thank the anonymous referee for comments that improved the presentation of this paper. MRS acknowledges the support of NASA GSRP grant NGT5-50339. This work was supported in part at Caltech by NSF AST-0096023, NASA NAG5-8506 and DoE DE-FG03-92-ER40701 and DE-FG03-88-ER40397.

## REFERENCES

- Abel T., Anninos P., Norman M. L., Zhang Y., 1998, *ApJ*, 508, 518  
 Abel T., Bryan G.L., Norman M.L., 2000, *ApJ*, 540, 39

- Agol E., Kamionkowski M., 2001, *MNRAS*, submitted (astro-ph/0109539)  
 Alcock C. et al., 2001, *ApJL*, 550, 169  
 Barkana R., Loeb A., 1999, *ApJ*, 523, 54  
 Barkana R., Loeb A., 2000, *ApJ*, 539, 20  
 Barkana R., Loeb A., 2001, *Physics Reports*, 349, 125  
 Bernstein R. A. Freedman W. L., Madore B. F., 2002, *ApJ*, 571, 107  
 Bond J. R., Carr B. J., Arnett W. D., 1986, *ApJ*, 306, 428  
 Bromm V., Coppi P. S., Larson R. B., 1999, *ApJ*, 527, L5  
 Bromm V., Coppi P. S., Larson R. B., 2002, *ApJ*, 564, 23  
 Bromm V., Ferrara A., Coppi P. S., Larson R. B., 2001a, *MNRAS*, 328, 969  
 Bromm V., Kudritzki R. P., Loeb A., 2001b, *ApJ*, 552, 464  
 Callaway J., 1985, *Phys. Rev. A*, 32, 775  
 Callaway J., Unnikrishnan K., Oza D. H., *Phys. Rev. A*, 36, 2576  
 Cambr esy L., Reach W. T., Beichman C. A., Jarrett T. H., 2001, *ApJ*, 555, 563  
 Carr B. J., Bond J. R., Arnett W. D., 1984, *ApJ*, 277, 445  
 Carr B., 1994, *ARA&A*, 32, 531  
 Cen R., 1992, *ApJS*, 78, 341  
 Ciardi B., Ferrara A., Marri S., Raimondo G., 2001, *MNRAS*, 324, 381  
 Couchman H. M. P., Rees M. J., 1986, *MNRAS*, 221, 53  
 Dwek E. et al., 1998, *ApJ*, 508, 106  
 Fryer C. L., Woosley S. E., Heger, A., 2001, *ApJ*, 550, 372  
 Eisenstein D. J., Hu W., 1999, *ApJ*, 511, 5  
 Elbaz D., Cesarsky C. J., Chaniai P., Aussel H., Franceschini A., Fadda D., Chary R. R., 2002, *A&A*, 384, 848  
 Ferland G. J., 1980, *PASP*, 92, 596  
 Haiman Z., Loeb A., 1997, *ApJ*, 483, 21  
 Hauser M. G., Dwek E., 2001, *ARA&A*, 39, 249  
 Heger, A., Woosley S. E., 2002, *ApJ*, 567, 532  
 Karzas W. J., Latter R., 1961, *ApJS*, 6, 167  
 Lacey C., Cole S., 1993, *MNRAS*, 262, 627  
 Loeb A., Rybicki G. B., 1999, *ApJ*, 524, 527  
 Madau P., Rees M. J., 2001, *ApJ*, 551, L27  
 Oh S.P., Nollett K.M., Madau P., Wasserburg G. J., 2001, *ApJ*, 562, L1  
 Osterbrock D. E., 1989, *Astrophysics of Gaseous Nebulae and Active Galactic Nuclei*. University Science Books, Sausalito, CA  
 Peebles P. J. E., 1993, *Principles of Physical Cosmology*. Princeton Univ. Press, Princeton, NJ  
 Press W. H., Schechter P., 1974, *ApJ*, 187, 425  
 Renault C., Barrau A., Lagache G., Puget J.-L., 2001, *A&A*, 371, 771  
 Schaerer D., 2002, *A&A*, 382, 28  
 Schneider R., Ferrara A., Natarajan P., Omukai K. 2002, *ApJ*, 571, 30  
 Seaton M. J., 1959, *MNRAS*, 119, 81  
 Storey P. J., Hummer D. G., 1995, *MNRAS*, 272, 41  
 Tegmark M., Silk J., Rees M.J., Blanchard A., Abel T., Palla F., 1997, *ApJ*, 474, 1  
 Totani T., Yoshii Y., Iwamuro F., Maihara T., Motohara K., 2001, *ApJL*, 550, 137  
 Wright E. L., Johnson B. D., 2001, submitted (astro-ph/0107205)